Final Report for

MONOLITHIC MICROWAVE INTEGRATED CIRCUIT DEVICES FOR ACTIVE ARRAY ANTENNAS

21 May 1983 to 20 August 1984

Grant No. NAG3-420

Prepared by

Professor R. Mittra

Electromagnetic Communication Laboratory
Department of Electrical and Computer Engineering
University of Illinois
1406 W. Green Street
Urbana, IL 61801

TABLE OF CONTENTS

Summary 1

1. CHARACTERIZATION OF MMIC DEVICES FOR ACTIVE ARRAY ANTENNAS 2

1.1. Introduction 2

1.2. Analysis of a Uniform Microstrip 5

1.3. Analysis of Discontinuities with Mode Matching . 13

2. CROSSTALK IN HIGH SPEED DIGITAL CIRCUITS AND INTERCONNECTIONS 17

2.1. Introduction 17

2.3. Transient Response 22

2.4. Application - Pulse Response Simulation 28

2.5. Conclusion 32

References 33

Summary

During this grant period we have investigated two different aspects of active antenna array design. The first of these involved the study of transition between monolithic microwave integrated circuits and rectangular waveguides. The second aspect of the study was concerned with the investigation of crosstalk in multiconductor transmission lines.

We have formulated the boundary value problem associated with a discontinuity in a microstrip line. This entailed, as a first step, the derivation of the propagating as well as evanescent modes of a microstrip line. We have completed this task and have also derived the solution to a simple discontinuity problem: change in width of the center strip. Currently, we are in the process of refining this solution.

As for the multiconductor transmission line problem, we have developed a computer algorithm for computing the crosstalk noise from the signal to the sense lines. The computation is based on the assumption that these lines are terminated in passive loads. During the next grant period we plan to generalize this program to the case where the lines are terminated by active logic gates.

1. CHARACTERIZATION OF MMIC DEVICES FOR ACTIVE ARRAY ANTENNAS

1.1. Introduction

During the past year, the University of Illinois has been involved in the study of transitions between monolithic microwave integrated circuits (MMIC's) and rectangular waveguide. This problem occurs in the design of active array antennas, where the gain and amplitude of the individual array elements are controlled by MMIC's. In this report, we will summarize the progress that has been made on this problem to-date.

Transitions between MMIC's and rectangular waveguides should have several properties. First, they should have a low insertion loss. Next, they should be structurally and thermally sound. Finally, these transitions should maintain the inherent reproducibility of the integrated circuit. A number of possible candidates for these transitions are shown in Figures 1 and 2. In order to determine which of these various transitions are likely to offer the best characteristics, it is necessary first to analyze them for insertion loss and return loss. We propose to achieve this by first breaking up a transition into a succession of abrupt discontinuities. If we can calculate the S-parameters of a single discontinuity, we should then be able to determine the characteristics of a cascade of such discontinuities. The purpose of this study will initially be to develop the tools necessary to study these abrupt discontinuities in printed circuits.

Abrupt printed circuit discontinuities may take a number of forms. The theory which is developed is general for many different types of discontinuities, as will be discussed later. For the present, however, it is necessary to begin by studying the most simple example of this discontinuity one can find. This turns out to be an abrupt change in the strip width of a shielded microstrip. A cross section of uniform shielded

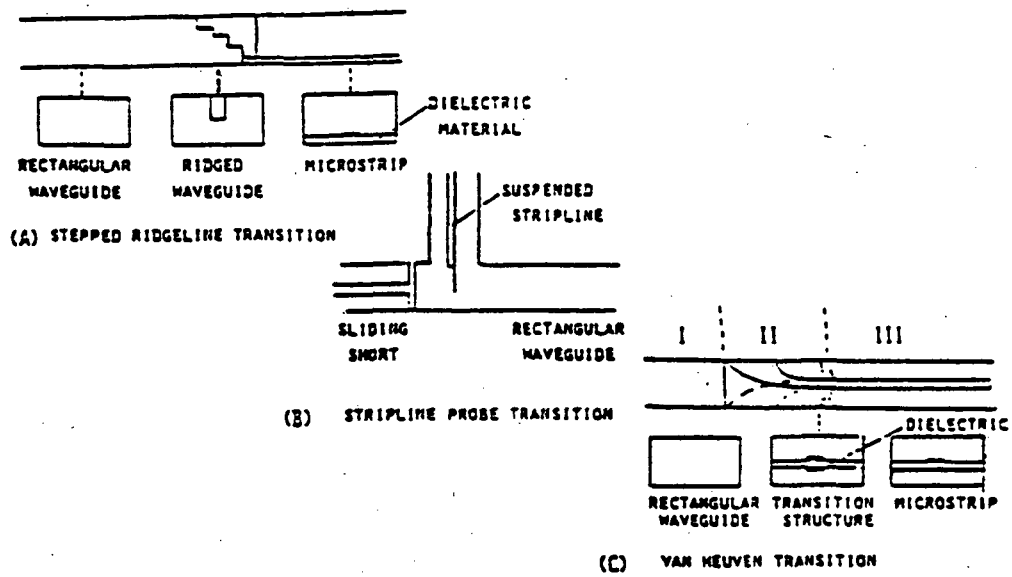

Figure 1. Typical substrate-to-waveguide transitions.

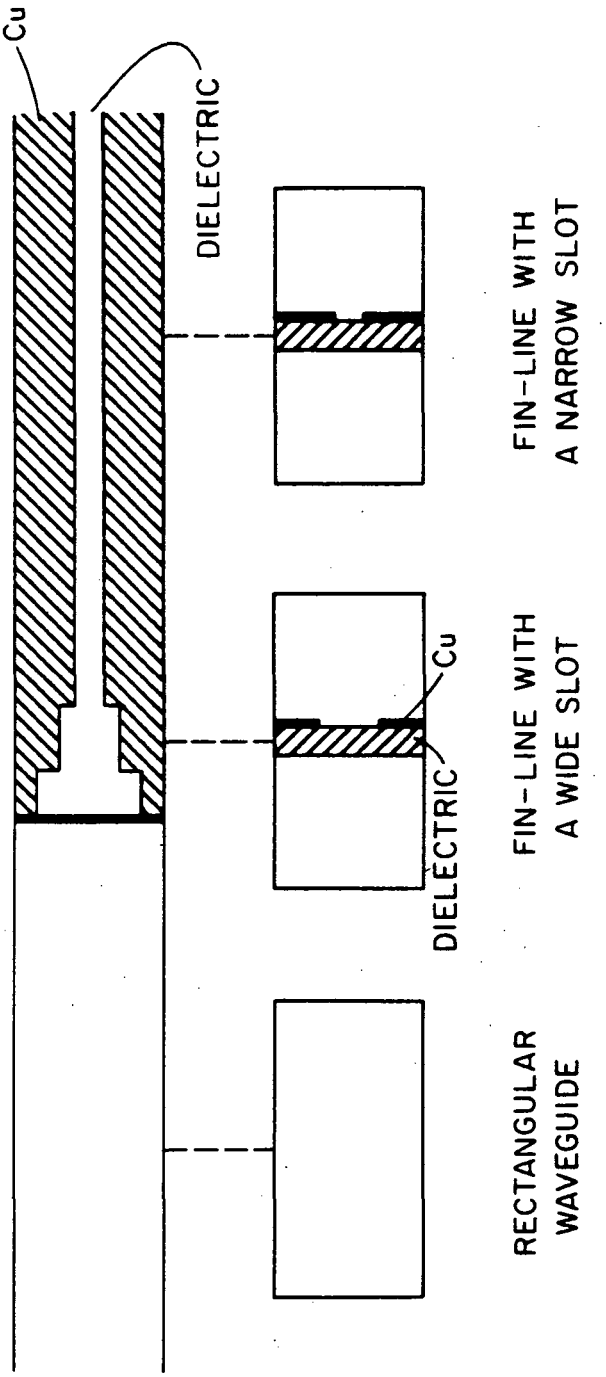

Figure 2. Transition between fin-line and rectangular waveguide.

microstrip is shown in Figure 3, and a discontinuity in the strip width is shown in Figure 4. By studying this structure, it is hoped that the tools necessary to study a more realistic transition, such as the fin-line stepped taper shown previously in Figure 2, will be developed.

The method to be used in the analysis of abrupt discontinuities involves mode matching in the plane of the discontinuity. In order to achieve this, one begins by generating the dominant and first few higher-order modes in each of the two microstrip lines. Next, one matches the tangential electric and magnetic field components in the plane of the discontinuity. Finally, one calculates the mode coefficients, which yield S-parameters and equivalent circuits of the discontinuity.

The study begins now with the analysis of the uniform microstrip.

1.2. Analysis of a Uniform Microstrip

The first step in the analysis of a uniform microstrip involves finding a Green's function which relates currents on the strip to the electric fields at all other points in the cross section of the line. This is accomplished by solving a two dimensional Helmholtz equation in regions I and II

$$(\nabla^2 + k_i^2) \begin{Bmatrix} \phi_i \\ \psi_i \end{Bmatrix} = 0 \tag{1.a}$$

$$k_i = \omega\sqrt{\mu_o \epsilon_i} \tag{1.b}$$

$$\epsilon_i = \begin{cases} \epsilon_i & x > 0 \\ \epsilon_i \epsilon_r & x < 0 \end{cases} \tag{1.c}$$

In the above equations, i denotes the region, and ϕ_i and ψ_i are the electric and magnetic scalar potentials in each region.

It is convenient to solve the above equation in the spectral domain, so one takes the Fourier transform of all potentials and fields as

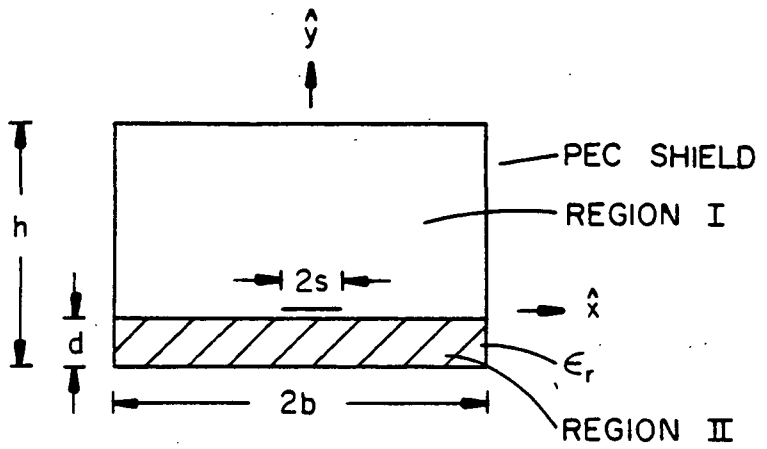

Figure 3. Cross section of shielded microstrip.

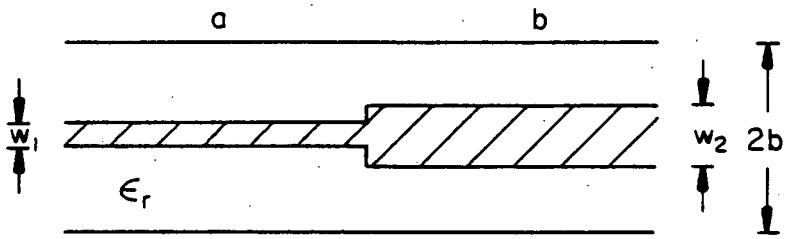

Figure 4. Top view of a discontinuity in the strip width on a microstrip.

$$\tilde{\phi}(n,y) = \int_{-\infty}^{\infty} \phi(x,y)\, e^{j\alpha_n x}\, dx \tag{2.a}$$

$$\phi(x,y) = \frac{1}{2b} \sum_{-\infty}^{\infty} \tilde{\phi}(n,y)\, e^{-j\alpha_n x} \tag{2.b}$$

$$\alpha_n = \frac{n\pi}{b} \tag{2.c}$$

By matching boundary conditions on the shield walls and on the center conductor, one obtains an equation of the form

$$\begin{bmatrix} Z_{zz}(\alpha_n,\beta) & Z_{zx}(\alpha_n,\beta) \\ Z_{xz}(\alpha_n,\beta) & Z_{xx}(\alpha_n,\beta) \end{bmatrix} \begin{bmatrix} J_z(\alpha_n) \\ J_x(\alpha_n) \end{bmatrix} = \begin{bmatrix} E_z(\alpha_n,\beta) \\ E_x(\alpha_n,\beta) \end{bmatrix} \tag{3}$$

This equation relates the current in the plane $y = 0$ to the electric fields in this plane. The dyadic Green's function, $Z_{ij}(\alpha_n,\beta)$, consists of relatively simple expressions in terms of hyperbolic sines and cosines.

Before proceeding to the solution of this equation for β, one should first look at the methods for generalizing the above Green's function. The above method is satisfactory for configurations with one dielectric layer and one strip. But a method developed by T. Itoh [1] gives a technique for generating a Green's function for structures with an arbitrary number of dielectric layers and conducting strips. His technique is called the Spectral Immitance Approach. While a detailed explanation of the technique is beyond the scope of this paper, it may be stated that the the technique involves the separation of the fields in each dielectric region into TE_y and TM_y components in the spectral domain, and the subsequent formulation of analogous transmission lines in the $\hat{y}$ direction for the decoupled TE and TM fields. This generalization extends the applicability of the techniques presented in this paper to a large class of printed circuits.

Next, one must find the solution to the integral equation shown in Equation (3).

The solution is effected by the spectral Galerkin technique [2], in which a moment method solution is brought about in the spectral domain. Hence, the current on the strip is expanded in terms of basis functions, which are non-zero only on the strip, as

$$J_z(x) = \sum_{i=1}^{N} c_i \frac{\cos\left((i-1)\pi(x/s)-1\right)}{\sqrt{1-(x/s)^2}} \tag{4.a}$$

$$J_x(x) = \sum_{i=1}^{N} d_i \frac{\sin\left(i\pi(x/s)-1\right)}{\sqrt{1-(x/s)^2}} \tag{4.b}$$

One then takes the Fourier transform of these currents and substitutes the result into Equation (3). Next, the inner product of the resulting equation is taken with the individual basis functions, and Parseval's theorem is used to eliminate the right-hand side. The resulting matrix equation may be solved by setting the determinant equal to zero and solving for β with Newton's method.

The accuracy of this method is determined by the number of basis functions and the number of spectral terms one can calculate within a reasonable amount of computer time. For the dominant mode and lower-order evanescent modes, a small number of basis functions and spectral terms is probably satisfactory. For evanescent modes of larger order, it is likely that more basis functions and spectral terms are required to achieve reasonable accuracy.

Sample calculations were carried out in order to calculate the dominant and first two evanescent modes of microstrip. These results are shown in Figure 5. One would like to compare these modes to other results, but little data are available on microstrip modes. The microstrip mode calculations that are available deal with propagating modes, but do not present data on evanescent modes [3][4]. There does exist, however, one paper which presents calculations of fin-line for both propagating and evanescent modes [5]. In order to adapt our analysis to fin-line, we need only change the dyadic Green's function, Z_{ij}. This was done, and a dispersion curve was

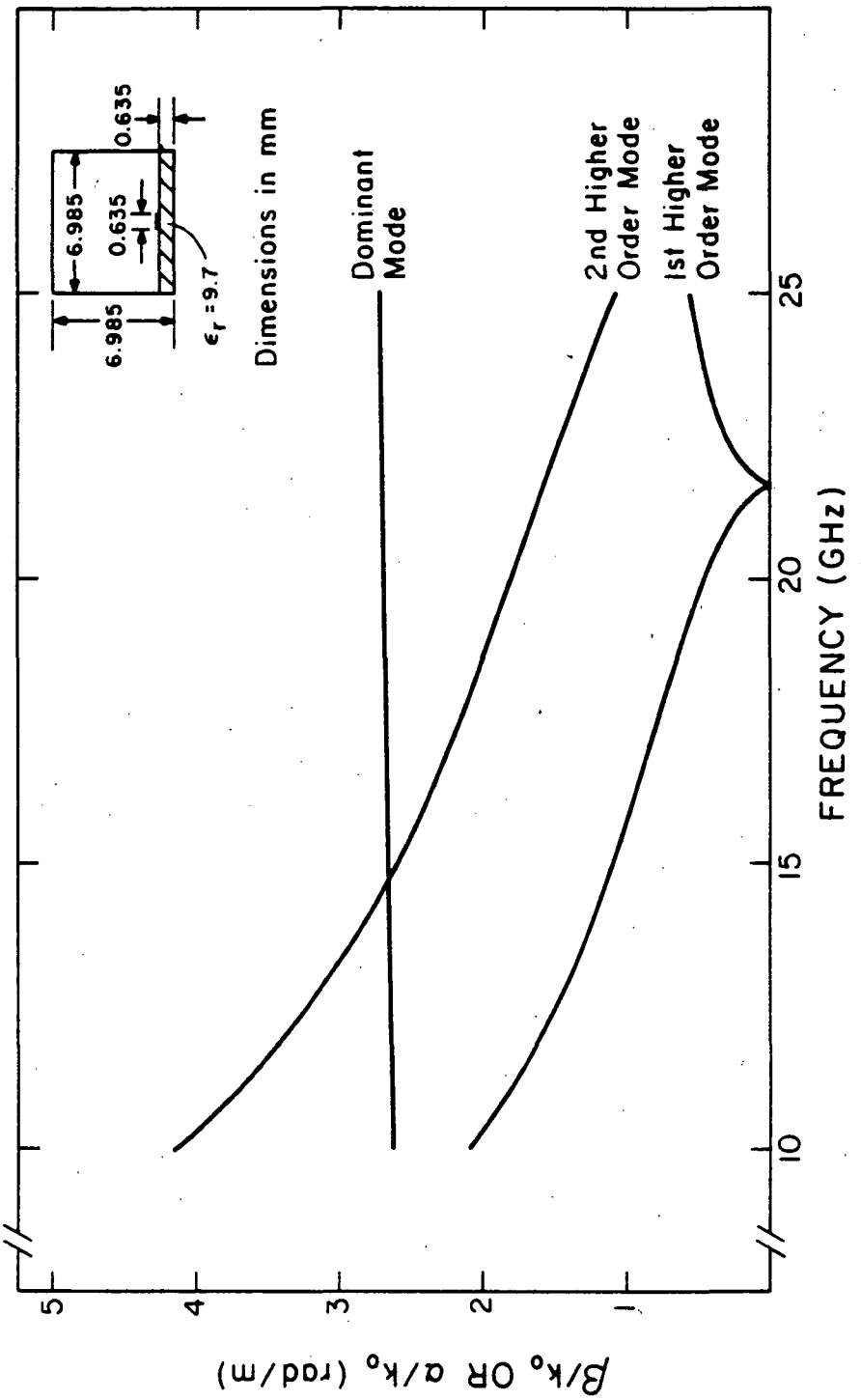

Figure 5. The dispersion characteristics of the dominant and first two even higher-order modes of microstrip. Two basis functions and 201 spectral terms were used.

calculated, which is shown in Figure 6. Clearly, satisfactory agreement with the results in Reference 5 has been achieved. Since the microstrip calculation is quite similar to the fin-line calculation, it is believed that the microstrip mode calculations should also be reasonable.

Once the modes have been found and verified, the next step is to calculate the characteristic impedance of the uniform line. This is done for two reasons. First, it gives added confirmation that the dominant mode calculation is accurate. Second, it gives a first-order approximation to the input impedance at a discontinuity. This result is useful as a comparison for results obtained with the mode matching technique. Since the characteristic impedance is defined only for TEM lines, one must be careful to choose a definition of characteristic impedance which is useful experimentally. The definition most commonly chosen is the power-current definition

$$Z_o = \frac{2P}{II^*} \tag{5.a}$$

$$P = \tfrac{1}{2}\,\mathrm{Re} \int\int E \times H^* \, dx \, dy \tag{5.b}$$

$$I = \int_{-s}^{s} J_z(x)\, dx \tag{5.c}$$

An alternative definition is the voltage-current definition

$$Z_o = \frac{V}{I} \tag{6.a}$$

$$V = -\int_{-d}^{0} E_y(y)\, dy \quad {}_{x=0} \tag{6.b}$$

Calculations were performed with both of these definitions, and are plotted in Figure 7. They correspond very well with data already published in Reference 4.

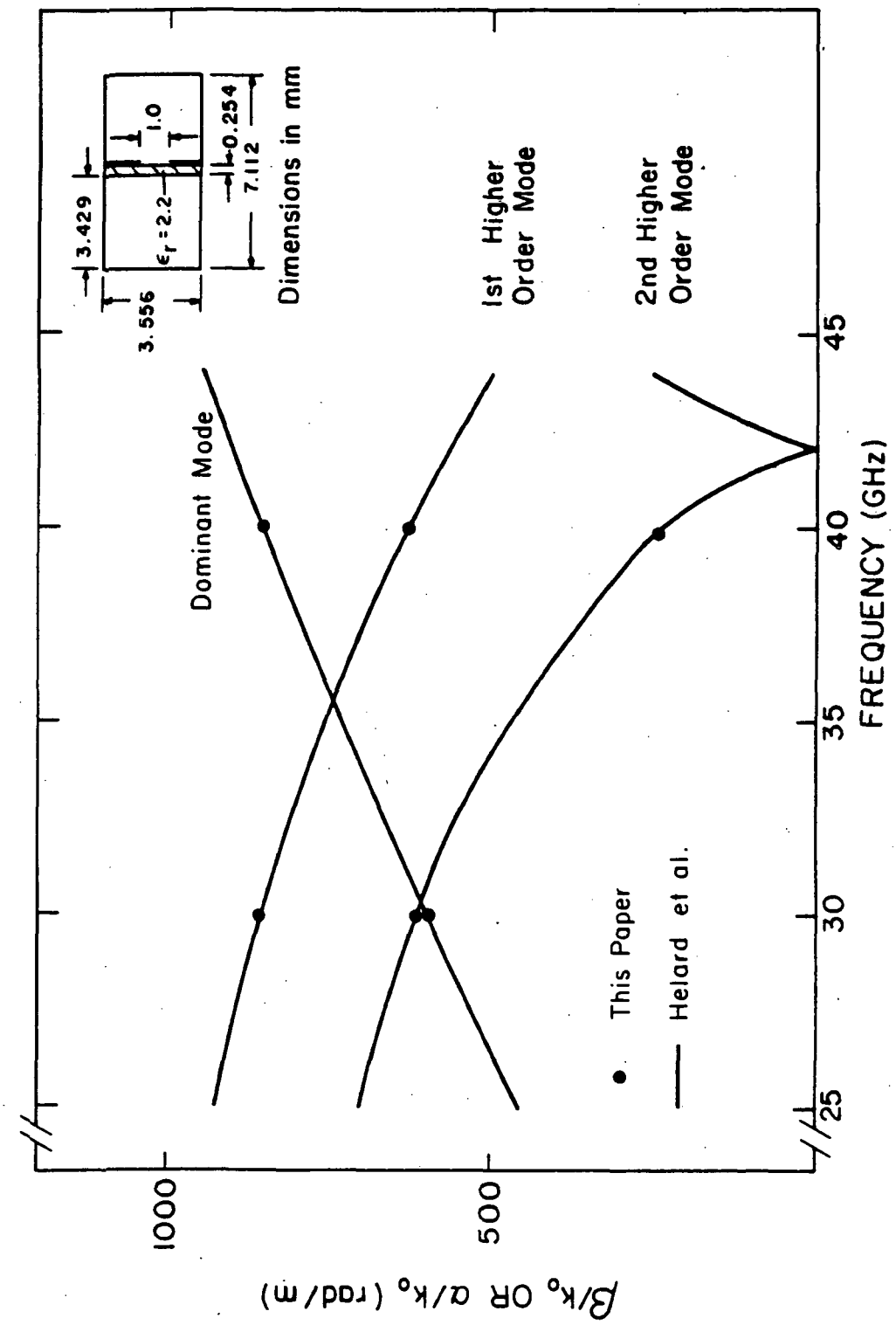

Figure 6. Dispersion curve of fin-line. Calculated with one basis function and 101 spectral terms.

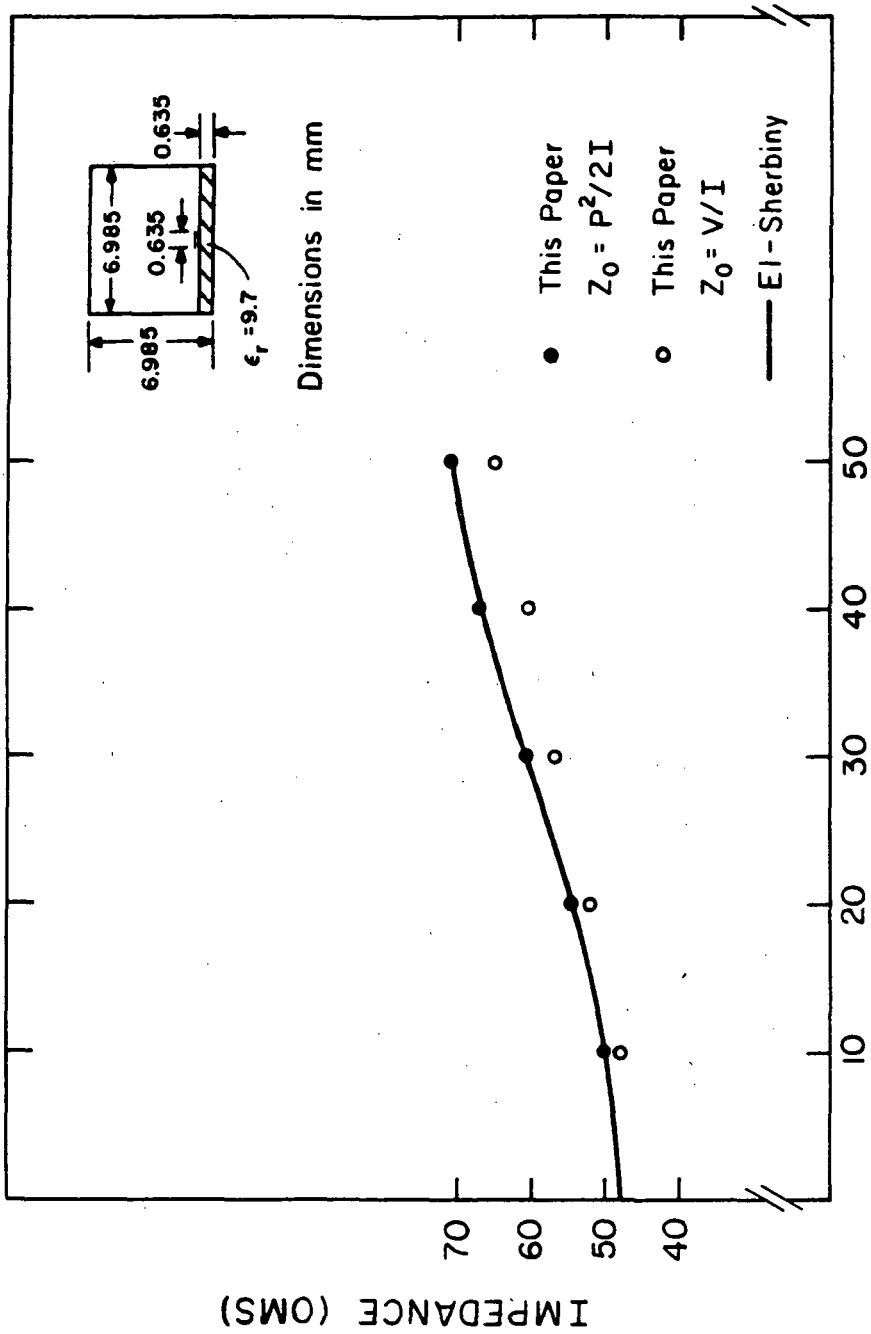

Figure 7. Characteristic impedance of microstrip using two definitions. Calculated with one basis function and 101 spectral terms.

1.3. Analysis of Discontinuities with Mode Matching

Among the techniques for studying waveguide discontinuities, mode matching seems one of the most promising [6]. This technique is suitable for calculating the characteristics of abrupt discontinuities, such as those in Figures 2 and 4. In addition, this method is easily adaptable to a cascade of abrupt discontinuities by using generalized S-parameters. Finally, it may be possible to model a smooth taper as a cascade of step discontinuities. Hence, the mode matching technique is capable of solving a wide variety of problems.

The mode matching technique begins by using the modes of the uniform microstrip calculated in the previous section. This involves finding the transverse fields for each mode and in each of the two waveguides,

$$\bar{e}_{ia}(n,y) = \tilde{e}_{xia}(n,y)\,\hat{x} + \tilde{e}_{yia}(n,y)\,\hat{y} \tag{7.a}$$

$$\bar{h}_{ia}(n,y) = \tilde{h}_{xia}(n,y)\,\hat{x} + \tilde{h}_{yia}(n,y)\,\hat{y} \tag{7.b}$$

where i denotes the mode number, and a denotes that we are referring to the input waveguide. Similar expressions hold for the output waveguide. At the point of the discontinuity, these transverse fields must be continuous. Enforcing this boundary condition, one obtains

$$(1+\rho)\,a_1\bar{e}_{a1} + \sum_{i=2}^{\infty} a_i\bar{e}_{ai} = \sum_{j=1}^{\infty} b_j\bar{e}_{bj} \tag{8.a}$$

$$(1-\rho)\,a_1\bar{h}_{a1} - \sum_{i=2}^{\infty} a_i\bar{h}_{ai} = \sum_{j=1}^{\infty} b_j\bar{e}_{bj} \tag{8.b}$$

where ρ is the reflection coefficient of the dominant mode, and a_i and b_j are the amplitudes of the modes in waveguides a and b, respectively. At this point, one takes appropriate inner products of Equation (8) and forms a matrix equation for ρ and for

the mode coefficients a_i and b_j. Once these have been found, equivalent circuit parameters, Z_n and Y_n, are calculated as shown in Figure 8. The circuit has now been characterized completely.

When using the above method, it is necessary to find an alternate method of calculating the equivalent circuit parameters. This gives approximate values for Z_n and Y_n, against which one can compare the results derived from the mode matching technique. The only alternate method in the literature which treats this problem uses a static technique, which is valid only for lower frequencies. An example of this technique is shown in Reference 7. Therefore, a lower frequency case was chosen for the initial study, in order to be able to compare the results with other sources. If the validity of the mode matching technique can be demonstrated at lower frequencies, one may assume the technique is valid also at higher frequencies.

By calculating a low frequency case, one is able to compare the results for Z_n and Y_n to calculations made with other methods. In this case, Z_n is approximated by the normalized characteristic impedance of waveguide 2, relative to waveguide 1. The power-current definition of characteristic impedance is used, as shown in Equation (5). Furthermore, one can get an approximation to Y_n by referring to the junction capacitances calculated in Figure 8.

A sample case of a microstrip discontinuity calculation is shown in Figure 8. The equivalent circuit parameters, Z_n and Y_n, are plotted as a function of the number of waveguide modes used. The convergence of the normalized input impedance, Z_n, to its correct value has been demonstrated. The input admittance Y_n, however, seems to be dependent upon the number of modes used in each guide. It is necessary to get Y_n to converge in order to obtain the junction capacitance. It is likely that improved convergence of Y_n can be obtained by improving the efficiency of the inner product calculation, thus allowing the use of more modes in the mode matching technique.

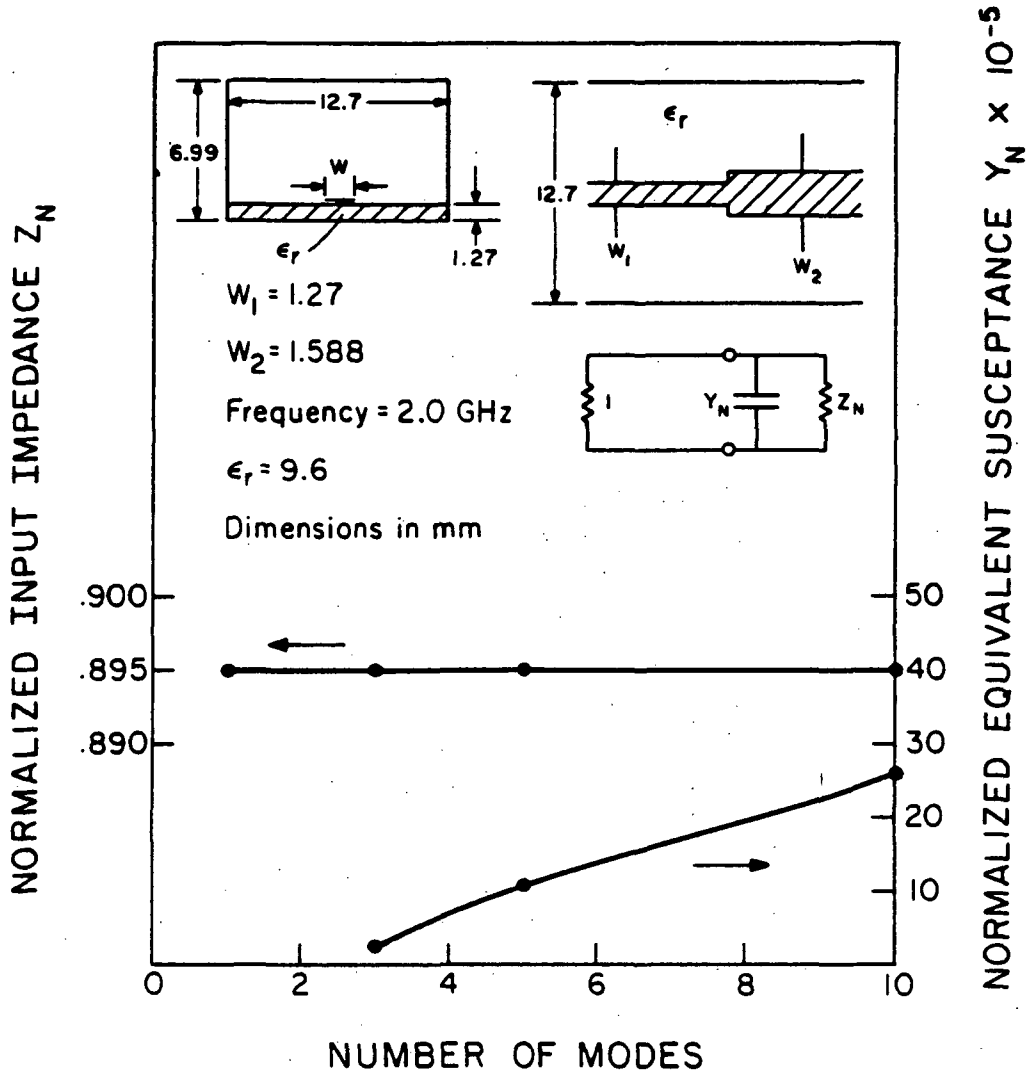

Figure 8. Variation of normalized input impedance and normalized susceptance with the number of waveguide modes. Calculated with one basis function and 101 spectral terms. It is expected that Z_n =0.985 and Y_n =128×10^{-5}.

There are many areas in this technique where additional study is needed. First, the sensitivity of the final answer to the number of spectral terms, the number of basis functions, and the number of modes used must be checked. Next, it is necessary to eliminate the dependency on the number of spectral terms used, by implementing an asymptotic form for the calculation of spectral terms of very large order. This change should reduce the computation time significantly. Finally, this technique should be applied to a variety of different structures such as those shown shown in Figures 1 and 2, and other structures useful in transitions between printed circuits and rectangular waveguides.

In summary a model for analyzing several types of transitions was described. The model involved the breakdown of transitions into a cascade of abrupt printed circuit discontinuities, whose S-parameters were determined with mode matching techniques. The initial results presented in this report demonstrate the method to be a promising one, although further work is still needed.

2. CROSSTALK IN HIGH SPEED DIGITAL CIRCUITS AND INTERCONNECTIONS

2.1. Introduction

The present trend toward high density packaging and the implemention of high speed digital devices have led to increasing demands for the characterization of the digital circuits and interconnections from the point of view of cross-talk and distortion of signal pulses propagating in these circuits. Our objective in this effort has been to develop models for predicting the coupling in multiconductor transmission lines and estimating the signal distortion due to mismatch in these lines. The signal corruption engendered by the cross-talk and the reflection due to terminations can introduce false logic levels and undesired triggering of logic gates. Hence an accurate estimation of the signal distortion and the noise is important in designing high speed digital circuits.

Since the introduction of electromagnetic couplers, several models for coupled lines have been proposed [8]. A frequency domain characterization [9] was performed using an integral equation technique to compute the capacitance and inductance matrix for coupled lines. Bryant and Weiss [10] established the relationship between the electrical and geometrical parameters of coupled microstrip pairs using the Green's function approach. Krage and Haddad [11], [12] determined the inductive and coupling coefficients as well as the directivity for various geometries of coupled lines. Hammerstad and Jensen [13] succeeded in implementing a model with errors less than that caused by physical tolerance and recently Kirshing and Jansen [14] reported reported frequency dependent expressions for microstrip pairs with excellent accuracy. Semiempirical equations for even and odd mode expressions for the design of such coupled structures were also derived [15]. Various authors extended the analysis to three-line couplers [16], [17] and, recently, Chan and Mittra [18] used a spectral-iterative technique based on the conjugate gradient method to compute the inductance

capacitance matrices of n-line microstrip structures.

In the prediction of signal propagation, early contributors [19]-[21] used a weak coupling approximation to predict the transient response in coupled pairs . Paul [22], [23] derived matrix chain parameter identities for the analysis of multiconductor transmission lines in the frequency domain for sinusoidal excitation. Using a similar technique, Zysman and Johnson [24] derived an equivalent circuit for two coupled lines. Chang [25] implemented a circuit model to describe the transient response of an n-conductor system using a congruence transformer approach. Such a model was implemented on CAD programs [26] to analyze the cross-coupling response of interconnections in high speed digital circuits. The above and several other equivalent circuit techniques have been proposed to describe terminal variables of multiconductor systems. However, no closed-form expression relating the transients to the position along the lines has been made available.

In the present study, we utilize the inductance and capacitance matrices of an n-line system terminated with passive linear impedances to derive the time- and position-dependent expressions for the transient response. The first step in our approach is to determine the modes of propagation of the network. Next, a Fourier integral analysis is applied to the system and the time-domain solutions are obtained. Finally, the accuracy of the method is evaluated by comparing the theoretical results with measurements.

2.2. Formulation - Natural Modes

The basic differential equations governing the propagation of voltages and currents in an n-line system can be written in a matrix form as

$$-\frac{\partial \mathbf{V}}{\partial x} = \mathbf{L}\frac{\partial \mathbf{I}}{\partial t} \tag{9}$$

$$-\frac{\partial \mathbf{I}}{\partial x} = \mathbf{C}\frac{\partial \mathbf{V}}{\partial t} \tag{10}$$

where **V** and **I** are column vectors of dimension n representing the line voltages and currents with $[\mathbf{V}]_{i1} = V_i$ and, $[\mathbf{I}]_{i1} = I_i$ which are the voltage and current on the *ith* line respectively. **L** and **C** are square matrices of dimension n representing inductance and capacitance per unit length respectively, with $[\mathbf{L}]_{ij} = L^{(s)}$ if $i = j$ and $[\mathbf{L}]_{ij} = L_i^{(m)}$ if $i = j$. $L^{(s)}$ is the self inductance per unit length of an isolated line and $L_i^{(m)}$ is the mutual inductance per unit length between *ith* and *jth* conductors. Similarly, $[\mathbf{C}]_{ij} = C^{(s)} + \sum_{k=1}^{n} C_{ik}^{(m)}\,(k=i)$ if $i = j$, and $[\mathbf{C}]_{ij} = -C_{ij}^{(m)}$ if $i = j$, where $C^{(s)}$ is the self capacitance per unit length of a single isolated line and $C_{ij}^{(m)}$, the mutual capacitance between *ith* and *jth* lines. These self and mutual parameters can be measured using TDR techniques [27]. Since the lines are identical, **L** and **C** are symmetric matrices. Equations (9) and (10) can be combined to yield

$$\frac{\partial^2 \mathbf{V}}{\partial x^2} = \mathbf{LC}\frac{\partial^2 \mathbf{V}}{\partial t^2} \tag{11}$$

$$\frac{\partial^2 \mathbf{I}}{\partial x^2} = \mathbf{CL}\frac{\partial^2 \mathbf{I}}{\partial t^2} \tag{12}$$

In general, **LC** and **CL** are not equivalent; moreover, **L** and **C** being symmetric does not imply that **LC** or **CL** are symmetric. However it is known [23] that there exist square matrices **E** and **H** which premultiply both sides of (11) and (12) to yield

$$\frac{\partial^2 \mathbf{EV}}{\partial x^2} = \mathbf{ELCE}^{-1}\frac{\partial^2 \mathbf{EV}}{\partial t^2} \tag{13}$$

$$\frac{\partial^2 \mathbf{HI}}{\partial x^2} = \mathbf{HCLH}^{-1} \frac{\partial^2 \mathbf{HI}}{\partial t^2} \tag{14}$$

where $\mathbf{ELCE}^{-1}$ and $\mathbf{HCLH}^{-1}$ are diagonal matrices of order n. Since $\mathbf{LC}$ is the adjoint matrix of $\mathbf{CL}$, it can be shown that

$$\mathbf{ELCE}^{-1} = \mathbf{HCLH}^{-1} = \Lambda_m^2 \tag{15}$$

Therefore (13) and (14) can be rewritten as

$$\frac{\partial^2 \mathbf{V_m}}{\partial x^2} = \Lambda_m^2 \frac{\partial^2 \mathbf{V_m}}{\partial t^2} \tag{16}$$

$$\frac{\partial^2 \mathbf{I_m}}{\partial x^2} = \Lambda_m^2 \frac{\partial^2 \mathbf{I_m}}{\partial t^2} \tag{17}$$

where

$$\mathbf{V_m} = \mathbf{EV} \tag{18}$$

$$\mathbf{I_m} = \mathbf{HI} \tag{19}$$

Equations (16) and (17) give the relations between the modal voltage and current matrices, $\mathbf{V_m}$ and $\mathbf{I_m}$. Λ_m is a diagonal eigenvalue matrix whose elements are given by $\{\Lambda_m\}_{ii} = 1/v_{mi}$, where v_{mi} is the velocity of propagation of the *ith* mode. The *ith* row of $\mathbf{E}$ and $\mathbf{H}$ are the voltage and current eigenvectors associated with the *ith* mode whose modal variables are given by $[\mathbf{V_m}]_{i1}$ and $[\mathbf{I_m}]_{i1}$ respectively. For the case where $\mathbf{L}$ and $\mathbf{C}$ are symmetric, there exist n distinct modes of propagation associated with n real eigenvalues and the set of linearly independent (real) eigenvectors forms a basis in n-dimensional space. In general, the entries of $\mathbf{E}$ and $\mathbf{H}$ depend on the entries of both $\mathbf{L}$ and $\mathbf{C}$. Otherwise, $\mathbf{E}$ and $\mathbf{H}$ are equivalent. The line variables can be recovered by using

$$\mathbf{I} = \mathbf{E}^{-1}\mathbf{V}_m \tag{20}$$

$$\mathbf{V} = \mathbf{H}^{-1}\mathbf{I}_m \tag{21}$$

If harmonic variation with time is assumed, the solutions to (16) and (17) have the form

$$\mathbf{V}_m(t,x) = \left| e^{-\frac{j\omega x}{v_m}}\mathbf{A} + e^{+\frac{j\omega x}{v_m}}\mathbf{B} \right| e^{j\omega t} \tag{22}$$

$$\mathbf{I}_m(t,x) = \mathbf{Z}_m^{-1}\left| e^{-\frac{j\omega x}{v_m}}\mathbf{A} - e^{+\frac{j\omega x}{v_m}}\mathbf{B} \right| e^{j\omega t} \tag{23}$$

where $e^{\pm\frac{j\omega x}{v_m}}$ is a diagonal matrix of order n with $[e^{\pm\frac{j\omega x}{v_m}}]_{ii} = e^{\frac{j\omega x}{v_{mi}}}$, ω is the angular frequency and $\mathbf{A}$ and $\mathbf{B}$ are modal coefficient column vectors of order n associated with the forward and backward waves respectively. Making use of these equations in (9) and (10) for forward and backward waves separately, one gets

$$\mathbf{Z}_m = \Lambda_m^{-1}\mathbf{E}\mathbf{L}\mathbf{H}^{-1} \tag{24}$$

$\mathbf{Z}_m$ is the modal impedance matrix (dimension n) which relates modal voltage and current waves. Analogously, a line or characteristic impedance matrix $\mathbf{Z}_c$ can be defined by requiring $\mathbf{V} = \mathbf{Z}_c\mathbf{I}$ for forward and backward waves separately. When combined with the above relations, one finds

$$\mathbf{Z}_c = \mathbf{E}^{-1}\mathbf{Z}_m\mathbf{H} = \mathbf{E}^{-1}\Lambda_m^{-1}\mathbf{E}\mathbf{L} \tag{25}$$

Since in general, $\mathbf{E}$ and $\mathbf{H}$ are not equivalent, $\mathbf{Z}_m$ and $\mathbf{Z}_c$ contain off-diagonal elements which account for the interdependence of modal and state variables.

2.3. Transient Response

The previous section presented the development of the expressions for the various matrices associated with a multiconductor transmission line system, the relationships between these matrices and the solution for a time-harmonic excitation. When the applied signals are arbitrary (nonsinusoidal, nonperiodic), the response will contain contributions from all frequencies. In this case, the coefficient vectors are functions of frequency and the time domain solutions for modal voltages and currents are obtained via integration in the frequency domain as follows:

$$\mathbf{V}_m(t,x) = \int_{-\infty}^{+\infty} \left[e^{-\frac{j\omega x}{v_m}} \mathbf{A}(\omega) + e^{+\frac{j\omega x}{v_m}} \mathbf{B}(\omega) \right] e^{j\omega t} d\omega \tag{26}$$

$$\mathbf{I}_m(t,x) = \mathbf{Z}_m^{-1} \int_{-\infty}^{+\infty} \left[e^{-\frac{j\omega x}{v_m}} \mathbf{A}(\omega) - e^{+\frac{j\omega x}{v_m}} \mathbf{B}(\omega) \right] e^{j\omega t} d\omega \tag{27}$$

The above equations can be rearranged in terms of the forward and backward voltage waves $\mathbf{V}_m^+$ and $\mathbf{V}_m^-$ to read

$$\mathbf{V}_m(t,x) = \mathbf{V}_m^+(t,x) + \mathbf{V}_m^-(t,x) \tag{28}$$

$$\mathbf{I}_m(t,x) = \mathbf{Z}_m^{-1} \left[\mathbf{V}_m^+(t,x) - \mathbf{V}_m^-(t,x) \right] \tag{29}$$

where

$$\mathbf{V}_m^+(t,x) = \int_{-\infty}^{+\infty} e^{-\frac{j\omega x}{v_m}} \mathbf{A}(\omega)\, e^{j\omega t} d\omega \tag{30}$$

$$\mathbf{V}_m^-(t,x) = \int_{-\infty}^{+\infty} e^{+\frac{j\omega x}{v_m}} \mathbf{B}(\omega)\, e^{j\omega t} d\omega \tag{31}$$

The matrix products $e^{-\frac{j\omega x}{v_m}}\mathbf{A}(\omega)$ and $e^{+\frac{j\omega x}{v_m}}\mathbf{B}(\omega)$ are the Fourier transforms of $\mathbf{V}_m^+$ and $\mathbf{V}_m^-$ respectively, and, therefore, satisfy the relations

$$e^{-\frac{j\omega x}{v_m}}\mathbf{A}(\omega) = \frac{1}{2\pi}\int_0^{+\infty} \mathbf{V}_m^+(t,x)\, e^{-j\omega t}\, dt \tag{32}$$

$$e^{+\frac{j\omega x}{v_m}}\mathbf{B}(\omega) = \frac{1}{2\pi}\int_0^{+\infty} \mathbf{V}_m^-(t,x)\, e^{-j\omega t}\, dt \tag{33}$$

We then apply the boundary conditions at $x=0$ and $x=l$ (see Fig. 9). This yields

$$\mathbf{Z}_s\mathbf{Z}_d^{-1}\mathbf{V}_s(t) = \mathbf{E}^{-1}\mathbf{V}_m(t,0) + \mathbf{Z}_s\mathbf{H}^{-1}\mathbf{I}_m(t,0) \tag{34}$$

$$\mathbf{0} = \mathbf{E}^{-1}\mathbf{V}_m(t,l) - \mathbf{Z}_L\mathbf{H}^{-1}\mathbf{I}_m(t,l) \tag{35}$$

$\mathbf{Z}_s$ and $\mathbf{Z}_L$ are the source and load impedance matrices respectively. They are constructed such that $[\mathbf{Z}_s^{-1}]_{ij} = (Z_i^{(sg)})^{-1} + \sum_{k=i}^{n} (Z_{ik}^{(sm)})^{-1}\,(k=i)$ if $i=j$, $[\mathbf{Z}_s^{-1}]_{ij} = -(Z_{ij}^{(sm)})^{-1}$ if $i=j$ and $[\mathbf{Z}_L^{-1}]_{ij} = (Z_i^{(Lg)})^{-1} + \sum_{k=i}^{n} (Z_{ik}^{(Lm)})^{-1}\,(k=i)$ if $i=j$, $[\mathbf{Z}_L^{-1}]_{ij} = -(Z_{ij}^{(Lm)})^{-1}$ if $i=j$. $\mathbf{Z}_d$ is a diagonal matrix with $[\mathbf{Z}_d]_{ii} = Z_i^{(sg)}$. $Z_i^{(sg)}$ and $Z_i^{(Lg)}$ are the resistances between *ith* line and ground at the source and load terminals respectively, whereas $Z_{ij}^{(sm)}$ and $Z_{ij}^{(Lm)}$ are the resistances between *ith* and *jth* lines at the source and load terminals respectively. $\mathbf{V}_s(t)$ is the column vector associated with the n arbitrary voltage sources at $x = 0$. A more general situation involving, in addition, voltage sources at the load terminals could be solved by using superposition and, hence, is not treated here. Taking the transforms of (34) and (35), and, using Eqs. (28)-(31), we obtain

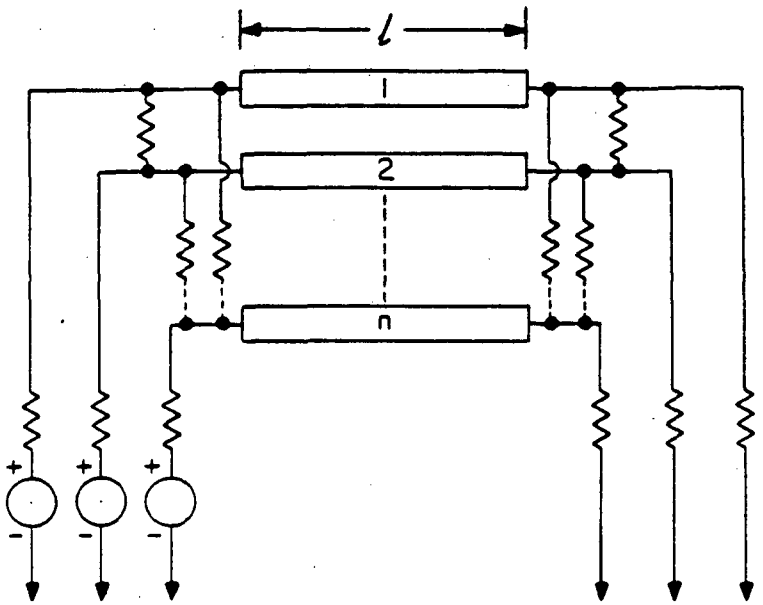

Figure 9. Schematic of an n-line multiconductor array.

$$\mathbf{Z_s Z_d^{-1} W_s(\omega) = E^{-1}\left[A(\omega) + B(\omega)\right] + Z_s L^{-1} E^{-1} \Lambda_m \left[A(\omega) - B(\omega)\right]} \tag{36}$$

$$\mathbf{0 = E^{-1}\left[e^{-\frac{j\omega l}{v_m}} A(\omega) + e^{+\frac{j\omega l}{v_m}} B(\omega)\right]}$$
$$\mathbf{- Z_L L^{-1} E^{-1} \Lambda_m \left[e^{-\frac{j\omega l}{v_m}} A(\omega) - e^{+\frac{j\omega l}{v_m}} B(\omega)\right]} \tag{37}$$

where $\mathbf{W_s}$ is the Fourier transform of $\mathbf{V_s(t)}$, defined by

$$\mathbf{W_s(\omega)} = \frac{1}{2\pi} \int_0^{+\infty} \mathbf{V_s(t)}\, e^{-j\omega t}\, dt \tag{38}$$

Equations (36) and (37) can be rearranged and combined to give

$$\mathbf{A(\omega) = \left[1_n - \Gamma_S e^{-\frac{j\omega l}{v_m}} \Gamma_L e^{-\frac{j\omega l}{v_m}} \right]^{-1} T W_s(\omega)} \tag{39}$$

$$\mathbf{B(\omega) = - e^{-\frac{j\omega l}{v_m}} \Gamma_L e^{-\frac{j\omega l}{v_m}} A(\omega)} \tag{40}$$

where $\mathbf{1_n}$ designates the unit matrix of order n. The matrices $\mathbf{\Gamma_S}$, $\mathbf{\Gamma_L}$ and $\mathbf{T}$ are respectively the source reflection coefficient, the load reflection coefficient and the transmission coefficient defined by

$$\mathbf{\Gamma_S = \left[1_n + E Z_s L^{-1} E^{-1} \Lambda_m \right]^{-1} \left[1_n - E Z_s L^{-1} E^{-1} \Lambda_m \right]} \tag{41}$$

$$\mathbf{\Gamma_L = \left[1_n + E Z_L L^{-1} E^{-1} \Lambda_m \right]^{-1} \left[1_n - E Z_L L^{-1} E^{-1} \Lambda_m \right]} \tag{42}$$

$$\mathbf{T = \left[1_n + E Z_s L^{-1} E^{-1} \Lambda_m \right]^{-1} E Z_s Z_d^{-1}} \tag{43}$$

As can be anticipated, if the lines are terminated at the load end with a network equivalent to the characteristic impedance of the system

($Z_L = Z_c = E^{-1}\Lambda_m^{-1}EL$. See Eqs. (24) and (25)), then $\Gamma_L = 0$ and no reflection occurs. This is the familiar result of the single line case. Such a situation can also be achieved with the source impedance network to eliminate re-reflections. In the general case where reflections occur at both ends, Γ_S and Γ_L are not diagonal, and Eqs. (39) and (40) cannot be simplified further. However, one can rewrite $A(\omega)$ in a geometric series† as

$$A(\omega) = \left| 1_n + \Gamma_S e^{-\frac{j\omega l}{v_m}} \Gamma_L e^{-\frac{j\omega l}{v_m}} + \left| \Gamma_S e^{-\frac{j\omega l}{v_m}} \Gamma_L e^{-\frac{j\omega l}{v_m}} \right|^2 + \cdots \right| TW_s(\omega) \qquad (44)$$

$$A(\omega) = \sum_{k=0}^{\infty} \left| \Gamma_S e^{-\frac{j\omega l}{v_m}} \Gamma_L e^{-\frac{j\omega l}{v_m}} \right|^k TW_s(\omega)$$

Making use of this relation, V_m^+ and V_m^- can be obtained using the inverse transform relations, (30) and (31)

$$V_m^+(t,x) = \delta(t-\frac{x}{v_m}) * \left| 1_n + \Gamma_S\delta(t-\frac{l}{v_m}) * \Gamma_L\delta(t-\frac{l}{v_m}) + \cdots \right| * TV_s(t)$$

$$= \delta(t-\frac{x}{v_m}) * \sum_{k=0}^{\infty} \left| \Gamma_S\delta(t-\frac{l}{v_m}) * \Gamma_L\delta(t-\frac{l}{v_m}) \right|^{k(*)} * TV_s(t) \qquad (45)$$

$$V_m^-(t,x) = -\delta(t-\frac{l-x}{v_m}) * \Gamma_L\delta(t-\frac{l}{v_m}) *$$

$$\sum_{k=0}^{\infty} \left| \Gamma_S\delta(t-\frac{l}{v_m}) * \Gamma_L\delta(t-\frac{l}{v_m}) \right|^{k(*)} * TV_s(t) \qquad (46)$$

In these expressions, $\delta(t-\frac{l}{v_m})$, $\delta(t-\frac{x}{v_m})$ and $\delta(t-\frac{l-x}{v_m})$ are diagonal matrices of order n with diagonal elements $[\delta(t-\frac{l}{v_m})]_{ii} = \delta(t-\frac{l}{v_{mi}})$, $[\delta(t-\frac{x}{v_m})]_{ii} = \delta(t-\frac{x}{v_{mi}})$ and $[\delta(t-\frac{l-x}{v_m})]_{ii} = \delta(t-\frac{l-x}{v_{mi}})$ respectively, $\delta(t-\tau)$ being the unit impulse function

† In a more rigorous manner,the necessary conditions for convergence of the geometric series must, a priori, be established. If the ratio for the series is diagonalizable, these conditions require that the magnitude of the associated eigenvalues be less than unity. In all cases however, convergence can be tested numerically before applying the geometric series expansion.

occurring at $t = \tau$. The symbol $*$ designates a convolution and the exponent $k(*)$ indicates that the term within brackets is being convolved with itself $k-1$ times, ($[f(t)]^{0(*)} = 1$ and $[f(t)]^{1(*)} = f(t)$). If we recall from transform theory

$$\delta(t-u) * \delta(t-v) = \delta(t-[u+v]) \tag{47}$$

$$\delta(t-u) * f(t) = f(t-u) \tag{48}$$

then the evaluations of (45) and (46) are reduced to a simple sequence of matrix multiplications in which the only time dependent factors are the delayed and attenuated versions of the applied signals represented by $\mathbf{V_s(t)}$. For an arbitrary time t, the voltages and currents are given by

$$\mathbf{V}(t,x) = \mathbf{E}^{-1}\left[\mathbf{V_m^+}(t,x) + \mathbf{V_m^-}(t,x)\right] \tag{49}$$

$$\mathbf{I}(t,x) = \mathbf{L}^{-1}\mathbf{E}^{-1}\Lambda_m\left[\mathbf{V_m^+}(t,x) - \mathbf{V_m^-}(t,x)\right] \tag{50}$$

In most practical cases, the source and load reflection cefficients are not very large; hence, only the first few terms of the infinite series need be retained in (45) and (46). However, in the event the mismatch is significant and the reflection coefficients are large, it becomes necessary to include more terms in the representation for $\mathbf{V_m^+}(t,x)$ and $\mathbf{V_m^-}(t,x)$. Equations (45) through (50) can be programmed on a computer to simulate the transient response of an n-line system for which the coupling parameters, the eigenvalues and the eigenvectors are known, and the terminations and the excitations are specified.

2.4. Application - Pulse Response Simulation

Many digital applications involve situations in which one or several transmission lines are excited with a pulse. Waveform distortions and cross-coupled signals are then observed at every point along the lines. In order to implement a realistic model for such phenomena, a four-line stripline structure (see Fig. 10) was fabricated on glass-epoxy (dielectric constant $\approx$ 4.5). The characteristic impedance of each line was designed to be 70 Ω. First the propagation characteristics were measured in order to determine the self and mutual parameters and set up inductance and capacitance matrices. The eigenvalues and eigenvectors associated with the matrix product **LC** were computed using an IMSL routine. Then, the lines were terminated as shown in Fig. 11 and the modal and state variables were computed using Eqs. (45)-(50). Finally the responses at $x = 0$ were plotted for each line and compared with the actual waveforms. As can be seen from Figs. 12 and 13, the agreement is very good within experimental errors. For the shown configuration, 4 iterations were needed to attain sufficient agreement. Other simulations were performed for microstrip as well as 7-line structures. In all cases, satisfactory agreement was obtained between theory and experiment.

The construction of the inductance and capacitance matrices requires the knowledge of the mutual parameters between any two conductors of the system. In practice, only the self and mutual parameters between adjacent lines need to be measured. Mutual coefficients between lines separated by another conductor can be approximated by extrapolation since they do not influence the response of the system significantly. From the geometry of these structures (microstrip and stripline) it can be anticipated that the mutual capacitance between two conductors decreases much faster than the mutual inductance as the number of conductors separating them and the spacing increase. This suggests that the cross-coupling in these multiconductor

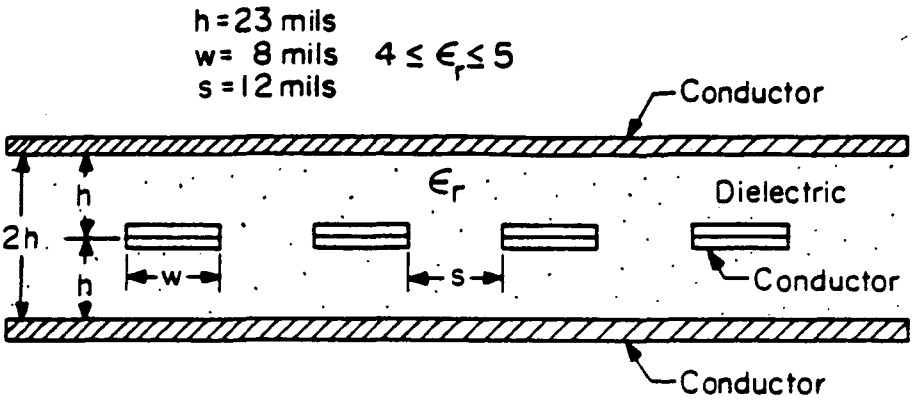

Figure 10. Cross-section of stripline test structure with four coupled lines.

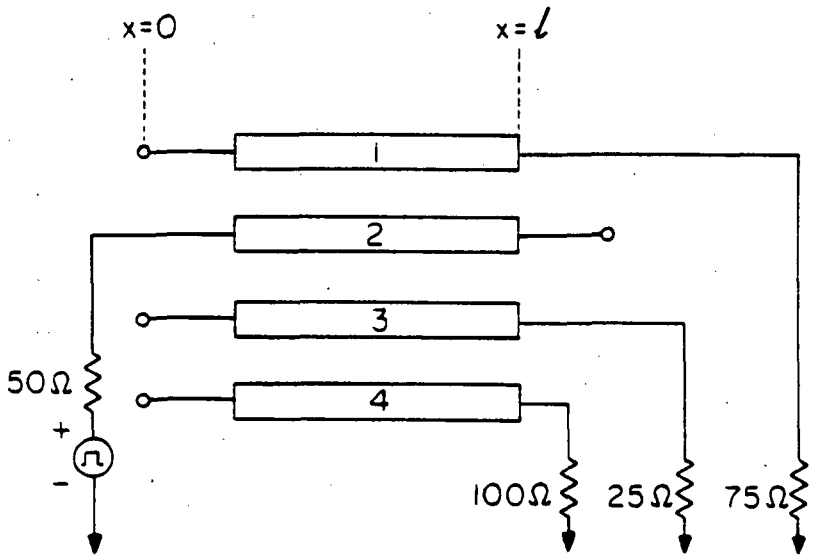

Figure 11. Schematic of 4-line coupler circuit used for experiment.

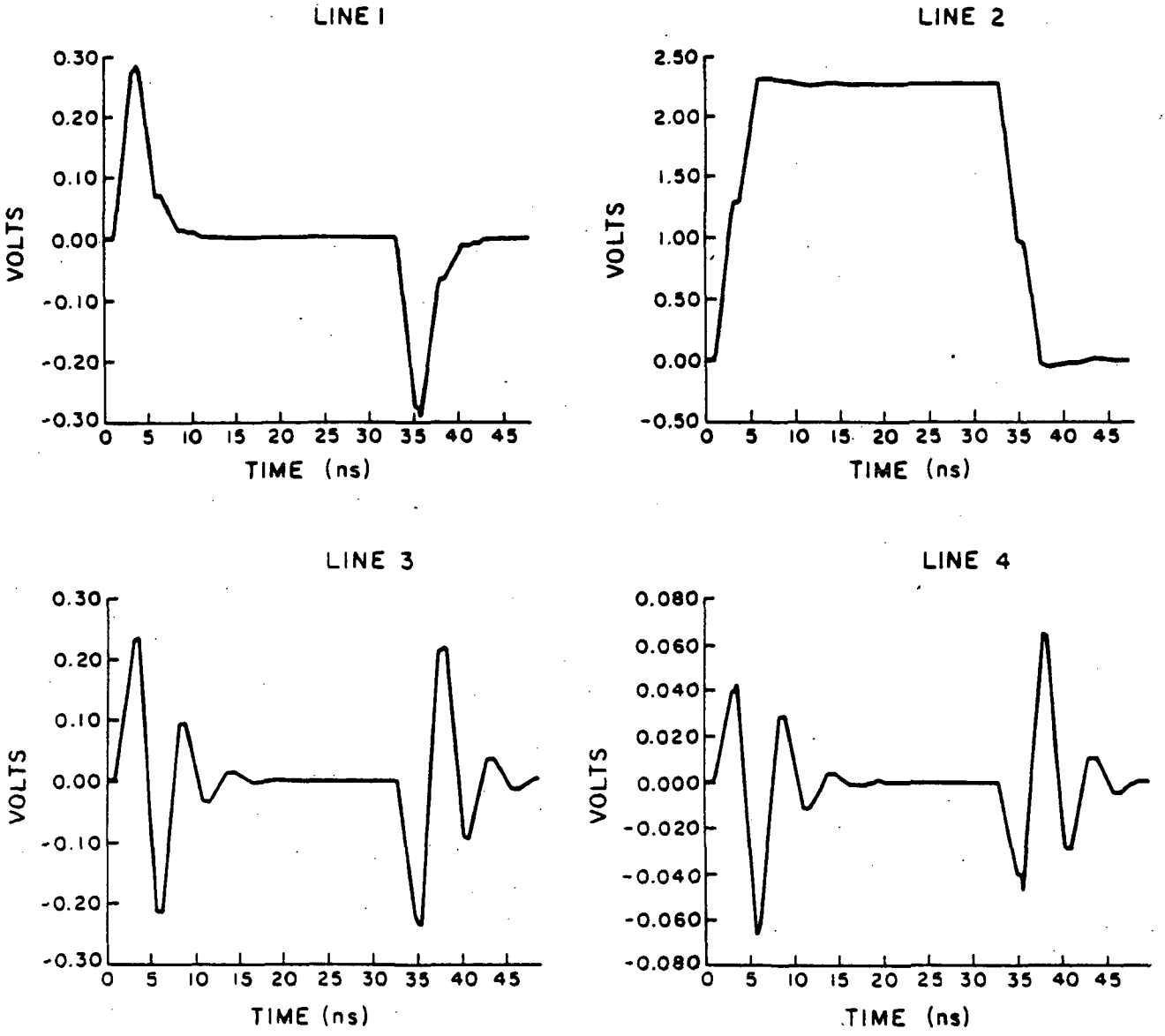

Figure 12. Simulated waveforms of the voltage at the near end ($x = 0$) for each line of the network of Fig. 11. Applied pulse magnitude: 2V, rise and fall time: 2 ns, pulse width: 30 ns.

LINE 1

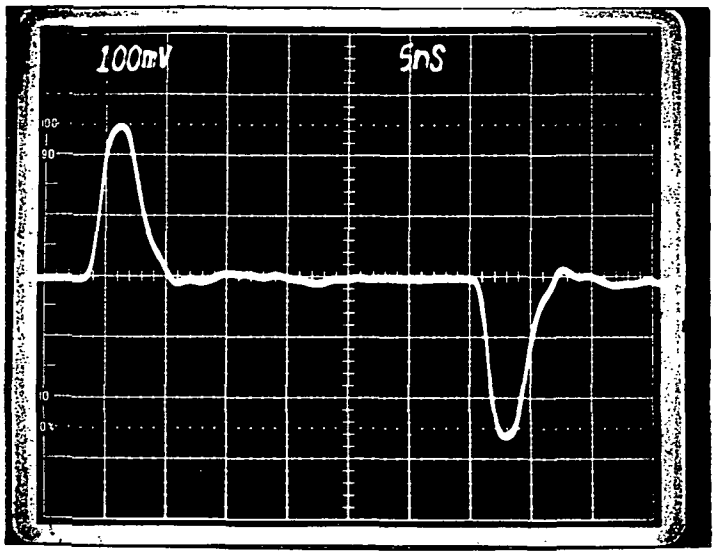

LINE 2

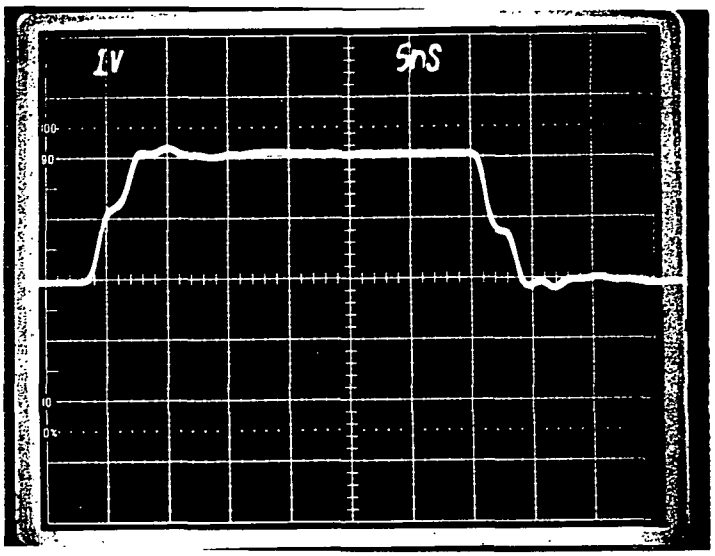

LINE 3

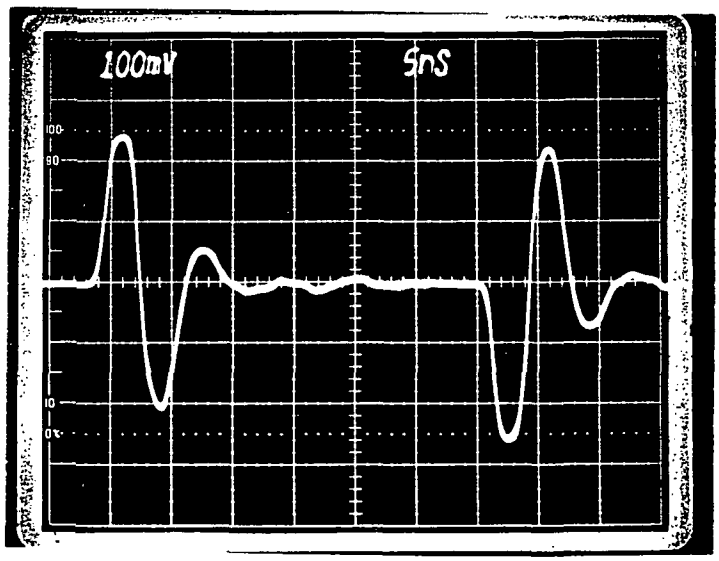

LINE 4

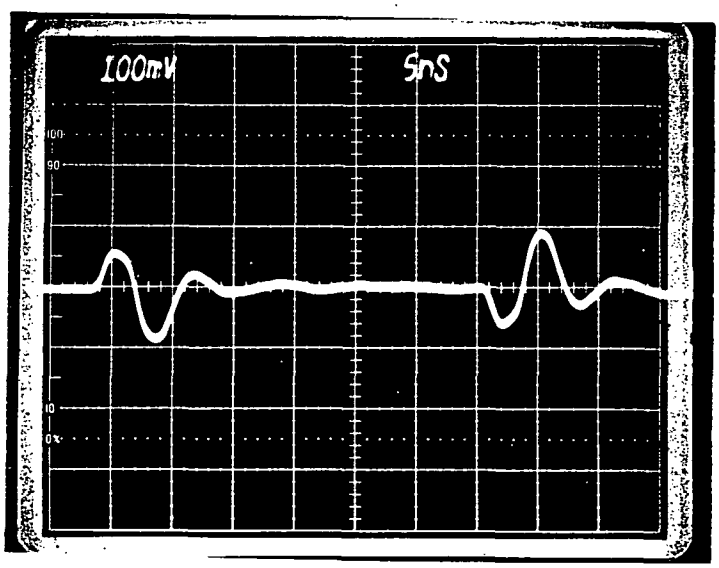

Figure 13. Experimental waveforms at $x=0$ observed at the near end of each line for the network of Fig. 11.

structures is predominantly inductive.

The preceding simulations also used pulses with rise times in the order of 1 nanosecond. The bandwidth associated with such speed is nearly 3 GHz. The variations of the line parameters were assumed to be negligible over this range. For much faster pulses however, the self and mutual coefficients become strong functions of frequency and the above analysis is no longer accurate. In this case the frequency dependence of the line parameters must be determined before using a numerical approach.

2.5. Conclusion

Simple closed-forms expressions for the propagation of transients in parallel conductors have been derived. These expressions describe the voltage and current at any point of a multiconductor system for which the coupling parameters are known. The analysis assumes that the terminations are real and passive and that the line parameters are invariant with frequency or time. Various experiments using pulse excitation were performed on microstrip and stripline structures and the agreement was found to be excellent for rise times and fall times less than one nanosecond.

References

1. Itoh, T. (1980) Spectral domain immitance approach for dispersion characteristics of generalized printed transmission lines, *IEEE Trans. Microwave Theory Tech.*, MTT-28:733-736.

2. Schmidt, L. and Itoh, T. (1980) Spectral domain analysis of dominant and higher order modes in fin-lines, *IEEE Trans. Microwave Theory Tech.*, MTT-28:981-985.

3. Mirshekar, D. and Davies, J. B. (1980) Accurate solution of microstrip and coplanar structures for dispersion and for dielectric and conductor losses, *IEEE Trans. Microwave Theory Tech.*, MTT-27:694-699.

4. El-Sherbiny, A. A. (1981) Accurate analysis of shielded microstrip lines and bilateral fin-lines, *IEEE Trans. Microwave Theory Tech.*, MTT-29:669-675.

5. Helard, M. et al. (1983) Exact calculations of scattering parameters of a step slot width discontinuity in a unilateral fin-line, *Electron. Lett.*, 19:537-539.

6. El-Hennawy, H. and Schuneman, K. (1983) Impedance transformation in fin-lines, *IEE Proc.*, 129:342-350.

7. Horton, R. (1973) Equivalent representation of an abrupt impedance step in microstrip line, *IEEE Trans. Microwave Theory Tech.*, MTT-21:562-564.

8. Oliver, B. M. (1954) Directional electromagnetic couplers, *Proc. IRE*, 42:1686-1692.

9. Kammler, D. W. (1968) Calculations of characteristic admittances and coupling coefficients for strip transmission lines, *IEEE Trans. Microwave Theory Tech.*, MTT-16:925-937.

10. Bryant, T. J. and Weiss, J. A. (1968) Parameters of microstrip transmission lines and of coupled pairs of microstrip lines, *IEEE Trans. Microwave Theory Tech.*, MTT-16:1021-1027.

11. Krage, M. K. and Haddad, G. I. (1970) Characteristics of coupled microstrip transmission lines-I : Coupled mode formulation of inhomogeneous lines, *IEEE Trans. Theory Tech.*, MTT-18:217-222.

12. Krage, M. K. and Haddad, G.I. (1970) Characteristics of coupled microstrip transmission lines-II : Evaluation of coupled line parameters, *IEEE Trans. Microwave Theory Tech.*, MTT-18:222-228.

13. Hammerstad E. and Jensen, O. (1980) Accurate models for microstrip computer-aided design, *IEEE MTT-S Int. Microwave Symp. Dig. (Washington, DC)*, 407-409.

14. Kirshing, M. and Jansen, R. (1984) Accurate wide-range design equations for the frequency-dependent characteristics of parallel coupled microstrip lines, *IEEE Trans. Microwave Theory Tech.*, MTT-32:83-90.

15. Garg, R. and Bahl, I. J. (1979) Characteristics of coupled microstrip lines, *IEEE Trans. Microwave Theory Tech.*, MTT-27:700-705.

16. Collier, R. and El Deeb, N. (1979) On the use of a microstrip three-line system as a six-port reflectometer, *IEEE Trans. Microwave Theory Tech.*, MTT-27:843-847.

17. Tripathi, V. K. (1977) On the analysis of symmetrical three-line microstrip circuits, *IEEE Trans. Microwave Theory Tech.*, MTT-25:726-729.

18. Chan, C. and Mittra, R. (1984) Spectral iterative technique for analyzing multiconductor microstrip lines, *IEEE MTT-S Int. Microwave Symp. Dig. (San Francisco, CA)*, 463-465.

19. Cotte, M. (1947) Theorie de la propagation d'ondes de choc sur deux lignes paralleles, *Revue Generale de l'Electricite*, 343-352.

20. Catt, I. (1967) Crosstalk (noise) in digital systems, *IEEE Trans. Electronic Computers*, EC-16:743-763.

21. Jarvis, D. B. (1963) The effects of interconnections on high-speed logic circuits, *IEEE Trans. Electronic Computers*, EC-12:476-487.

22. Paul, C. R. (1975) Useful matrix chain parameter identities for the analysis of multiconductor transmission lines, *IEEE Trans. Microwave Theory Tech.*, MTT-23:756-760.

23. Paul, C. R. (1974) On uniform multimode transmission lines, *IEEE Trans. Microwave Theory Tech.*, MTT-22:454-457.

24. Zysman, G. I. and Johnson, A. K. (1959) Coupled transmission line networks in an inhomogeneous dielectric medium, *IEEE Trans. Microwave Theory Tech.*, MTT-17:753-759.

25. Chang, F.Y. (1970) Transient analysis of lossless coupled transmission lines in a nonhomogeneous dielectric medium, *IEEE Trans. Microwave Theory Tech.*, MTT-18:616-626.

26. Chang, F. Y. (1980) Computer-aided characterization of coupled TEM transmission lines, *IEEE Trans. Circuits Syst.*, CAS-27:1194-1205.

27. Schutt-Aine, J. (1984) Analysis of pulse propagation on coupled microstrip transmission lines, Master's Thesis, University of Illinois, Urbana.